To appear in *Advanced Robotics*
Vol. 00, No. 00, October 2020, 1–16

FULL PAPER

Control of a snake robot for passing through a self-closing door

Mizuki Nakajima[a]*, Motoyasu Tanaka[a], and Kazuo Tanaka[a]

[a]*Department of Mechanical and Intelligent Systems Engineering, The University of Electro-Communications, 1-5-1 Chofugaoka, Chofu, Tokyo, Japan*;

(*v1.0 released October 2020*)

We propose the control method for a snake robot to pass through a self-closing door. The proposed method is realized by applying the two-point simultaneous control method. The position and orientation of head and tail of the robot are controlled simultaneously by using the two-point simultaneous control method. By controlling the position and orientation of the head of the robot, the robot opens the door and keeps it open. At the same time, the robot enters through the door from the tail by controlling the tail of the robot simultaneously. The robot passes through the door by pushing away the side of the door with the body. The proposed method enables the robot to enter the interior separated by a door and contributes to the expansion of the activity environment for snake robots. The experimental result validates the proposed methods.

Keywords: Biologically-Inspired Robots, Motion Control, Redundant Robots, Snake Robot.

1. Introduction

The snake robot that mimics snakes can propel on various environments by utilizing its elongated body shape and a high degree of freedom. It has multiple joints, which makes it difficult for the operator to directly control the joint angles. Therefore, researchers have focused on the motion control for the robot. By observing and analyzing the motion of snakes, Hirose formulated the lateral undulation of the snake as a serpenoid curve and realized the propulsion of the snake robot on the plane [1]. Several studies have realized the robot propulsion by generating periodic bending motions using the central pattern generator (CPG), the neural circuit that controls the cyclic movement of the organism: the motion on slope with the online optimization of the undulation based on CPG [2] and the avoidance of collision by the propulsion direction control based on the sensor information [3].

Studies into control methods for snake robot motion have proposed heuristic methods such as the representation of robot body shape as continuous curves. Yamada et al. proposed the method to control the joints of the robot with low computational cost. The body shape followed the target continuous curve, and the articulated mobile robot realized traversing the steps by changing the target curve as sending waves [4]. Kamegawa et al. have realized the propulsion on a pipe by controlling the body shape of the robot so as to coil around the pipe and rotating the robot around its trunk axis [5]. This method has been applied to propulsion on bent pipes [6] and branched pipes [7]. Takemori et al. generated complex target continuous curve by concatenating simple continuous curves, and have realized traversing on uneven terrain [8] and climbing a ladder [9]. Hatton and Choset have proposed representing the gait of the robot as the repetition of several characteristic body shapes and realized locomotion by transiting between them smoothly

*Corresponding author. Email: mizuki.nakajima@rc.mce.uec.ac.jp

[10]. Several studies control the motion of the robot by determining the joint angles based on the gait function, which represents the motion of the robot as the periodic motion of the joints. Rollinson and Choset realized locomotion in pipes connected at right angles and locomotion on the pipes combining different diameter pipes, by modifying the gait parameters based on the robot's joint angles and adapting the robot to the environment [11]. Gong et al. have proposed the method that realized the locomotion on various slopes by changing the gait parameter with the estimated slope angle automatically [12].

Several researchers formulate the frictional characteristics of snakes and utilize the high degree of freedom to snake robots. Compared to others, these methods allow for better control of the robot's position and orientation explicitly using the robot's redundancy. Several studies treat the frictional characteristics of snakes as velocity constraints by wheels, while others treat it as anisotropic friction. The methods using the former have realized the arbitrary trajectory tracking of the head of the robot on a plane [13] and the three dimensional trajectory tracking [14]. The singular configuration avoidance [15] and the collision avoidance [16] is possible through the utilization of the robot's redundancy. In addition, the proposed active switching of the velocity constraint by lifting the wheel slightly enhance the avoidance of moving obstacle [17] and the body shape changes without moving the head [18]. Based on the model using the anisotropic friction, the path following control of the robot's center of gravity [19] and the obstacle-aided locomotion [20, 21], where the obstacles are actively pushed by the robot, have been proposed.

Recently, performing works by the robot are being studied: grasping objects and valve operation with the soft gripper attached to the head of the robot [22], and valve operation in the water [23]. In these studies, the robot behaves as a mobile manipulator and performs tasks by controlling the position and orientation of the head of the robot. We proposed the simultaneous control of two points for the snake robot [24], and realized several works by making it behave as a dual arm manipulator, such as caging transportation and steering a cart. By applying this control method, we have also proposed the action of passing through a self-closing door by simultaneously controlling the head and tail of the robot [25]. However, the effectiveness of the proposed motion was verified by simulations, not experiments. In addition, sometimes the robot failed to pass through the door by collision with the edge of the door and the wheels of the robot.

In this paper, we are working on the realization of passing through a simple self-closing door using the actual robot. In addition, we prevent the robot from the stuck which is caused by the collision between the edge of the door and the wheel of the robot by making the outer shape of the robot smooth. By using the proposed method, a robot can enter the interior separated by a door. The proposed method will contribute to the expansion of the activity environment for snake robots.

2. Problem Setting

Figure 1 shows the assumed environment. We assume the door to be a miniaturized pulling door. Outside is defined as the side where the robot is positioned, whereas inside is the other side of the door. The door opens by pulling a knob attached to the outside of the door and closes automatically by the spring attached to the hinge when the knob is released. The door is assumed to be tall enough for the robot to pass through and avoid collision between the robot and the top of the door. The axis of rotation of the door is parallel to the normal vector of the ground. Walls are set on the either side of the door so that the robot cannot avoid the door to pass through. The environment is assumed to be an unknown environment, and the absolute position and orientation of the door and robot are not measurable.

Figure 2 shows a schematic of the snake robot. Fig. 2(a) and Fig. 2(b) show schematics of the motion on a plane and head raising motion, respectively. The snake robot consists of $2n$ links connected in series by rotational joints. Let l be the length of each link. The yaw and

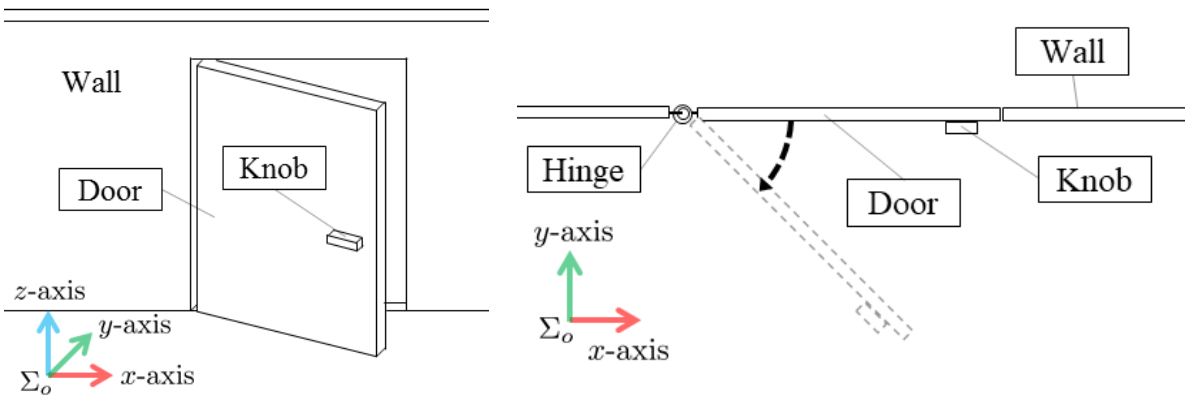

(a) Isometric view (b) Top view

Figure 1. The self-closing door

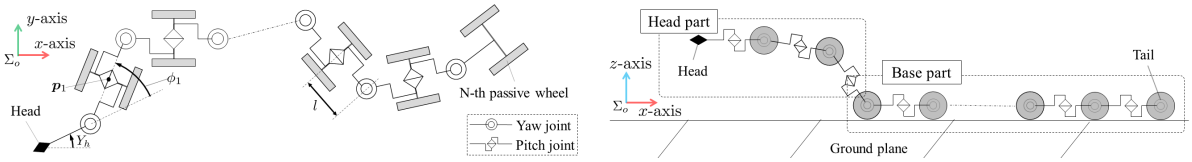

(a) Top view (b) Side view

Figure 2. The snake robot

pitch joints are alternately attached as shown in Fig. 2(a). Let $\boldsymbol{\psi} \in \mathrm{R}^{2n-1,1}$ and $\boldsymbol{\phi} \in \mathrm{R}^{n,1}$ be the vectors of all joint angles and the vectors of all yaw joint angles, respectively. The robot realizes three dimensional movement by using these joints. n pairs of passive wheels are attached coaxially to the tail and the pitch joints of the robot. Using the anisotropic friction of the passive wheel, propulsion is achieved by undulating the body. The joint structure is similar to previous studies, and the robot can realize three dimensional trajectory tracking by raising its head [14, 22], body shape approximation to a continuous curve [4], or more. In addition, a simple hook to pull the knob is attached to the head of the robot. Three dimensional motion is possible by lifting the wheels near the head [14], as shown in Fig. 2(b). We call the part where the robot touches the ground, the *base part*, and the part from the head to the base part, the *head part*. Let n_h and n_b be the number of wheels of the head part and the base part, respectively. The joints of the head part are from the first joint to the pitch joint coaxial to the first base part wheel. Similarly, the joints of the base part are from the yaw joint behind the first wheel of the base part to the tail joint. Let $\boldsymbol{\psi}_h \in \mathrm{R}^{2n_h+2,1}$ be the joint angles of the head part, $\boldsymbol{\psi}_b \in \mathrm{R}^{2n_b-3,1}$ be the joint angles of the base part, and $\boldsymbol{\phi}_b \in \mathrm{R}^{n_b-1,1}$ be the yaw joint angles of the base part. In addition, let $\boldsymbol{p}_h = \left[x_h, y_h, z_h, R_h, P_h, Y_h\right]^\top$ be the position and orientation of the head, $\boldsymbol{p}_t = \left[x_t, y_t, z_t, R_t, P_t, Y_t\right]^\top$ be the position and orientation of the tail, and $\boldsymbol{q} = \left[\boldsymbol{p}_h^\top, \boldsymbol{\psi}^\top\right]^\top \in \mathrm{R}^{2n+5,1}$ be the generalized coordinates.

The purpose of this study is for the snake robot to open a self-closing door and pass through it. By using a gripper that is attached to the head of the robot, grasping an object and manipulating valves can be realized [22]. Opening the door by this approach has been verified. When the door opens by pushing, the robot can use the previous method to pass through. In contrast, when the

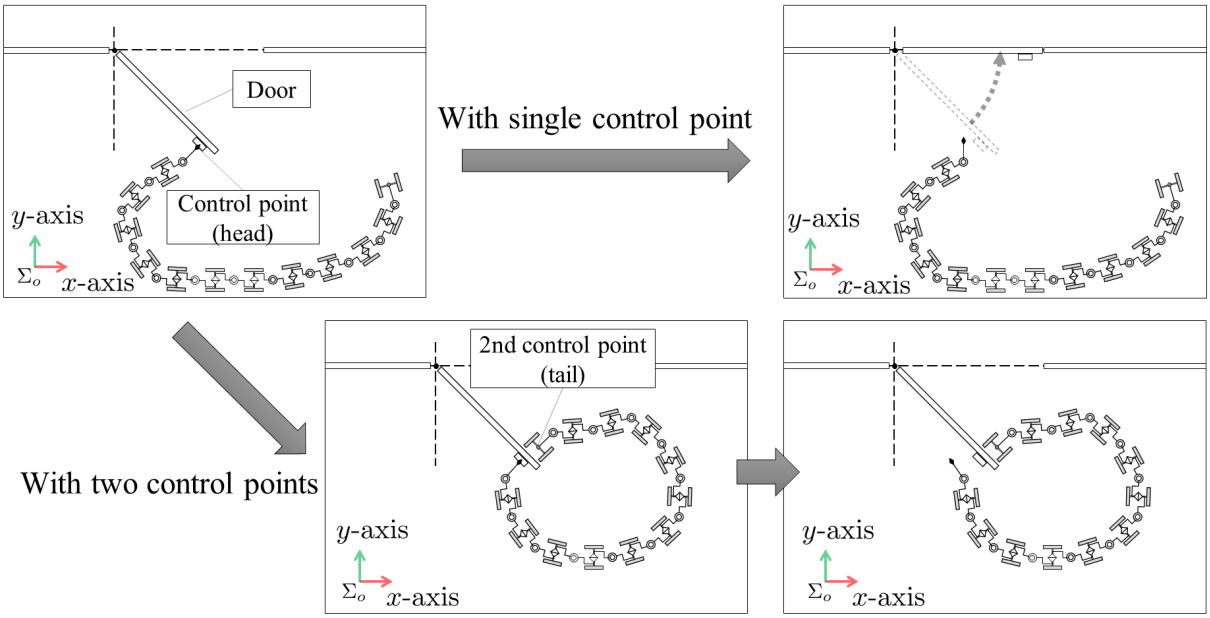

Figure 3. Overview of the proposed motion

door requires pulling, it is impossible for the robot to pass through using the previous method, which controls the position and orientation of a single point, since the door closes when the knob is released as shown in Figure 3. In order to pass through the self-closing door, it is necessary to devise a way for keeping the door open. Motion design for mobile manipulator to pass through a self-closing door has been proposed in [26, 27]. The motion for the wheelchair which has a manipulator have been proposed in [26], and the motion for the crawler-type mobile manipulator have been proposed in [27]. In [26], the door is prevented from closing by the wheelchair, moved inside after opening the door. In [27], the flipper of the robot is placed inside to prevent the door from closing. These robots have some mechanism for opening the door, such as a manipulator, and the door is kept open by using these mechanisms. Then, the robot passes through the door by moving the robot body while keeping the door open. However, it is difficult to equip a snake robot with such a mechanism, and these methods cannot be applied.

In this paper, we apply the two-point simultaneous control method [24] and aim to pass through a self-closing door by having the robot behave like a mobile two-armed manipulator. By controlling the head and tail of the robot simultaneously as shown in Fig. 3, the robot prevents the door from closing. We have proposed the outline of the motion for passing through the door in [25], and demonstrated the validity of the proposed motion in the simulation. However, verification by an actual robot was not conducted. In addition, sometimes the robot failed to pass through the door by collision with the edge of the door and the wheels of the robot. Therefore, in this study, we make the body shape of robot smooth and prevent from colliding the edge of the door and the wheel of the robot.

3. Motion Design

Figure 4 shows the overview of the proposed motion consisting of three parts. First, the robot pulls the knob by the hook which is mounted on the head and opens the door (Figure 4(a)). By controlling the three dimensional position and orientation of the head, the hook is hung on the knob, and the door is pulled open by the hook. The robot then enters the inside of the door while keeping the door open by controlling the head and tail simultaneously (Figure 4(b)). The door is kept open by pulling the knob by the hook, and the robot enters inside of the door through

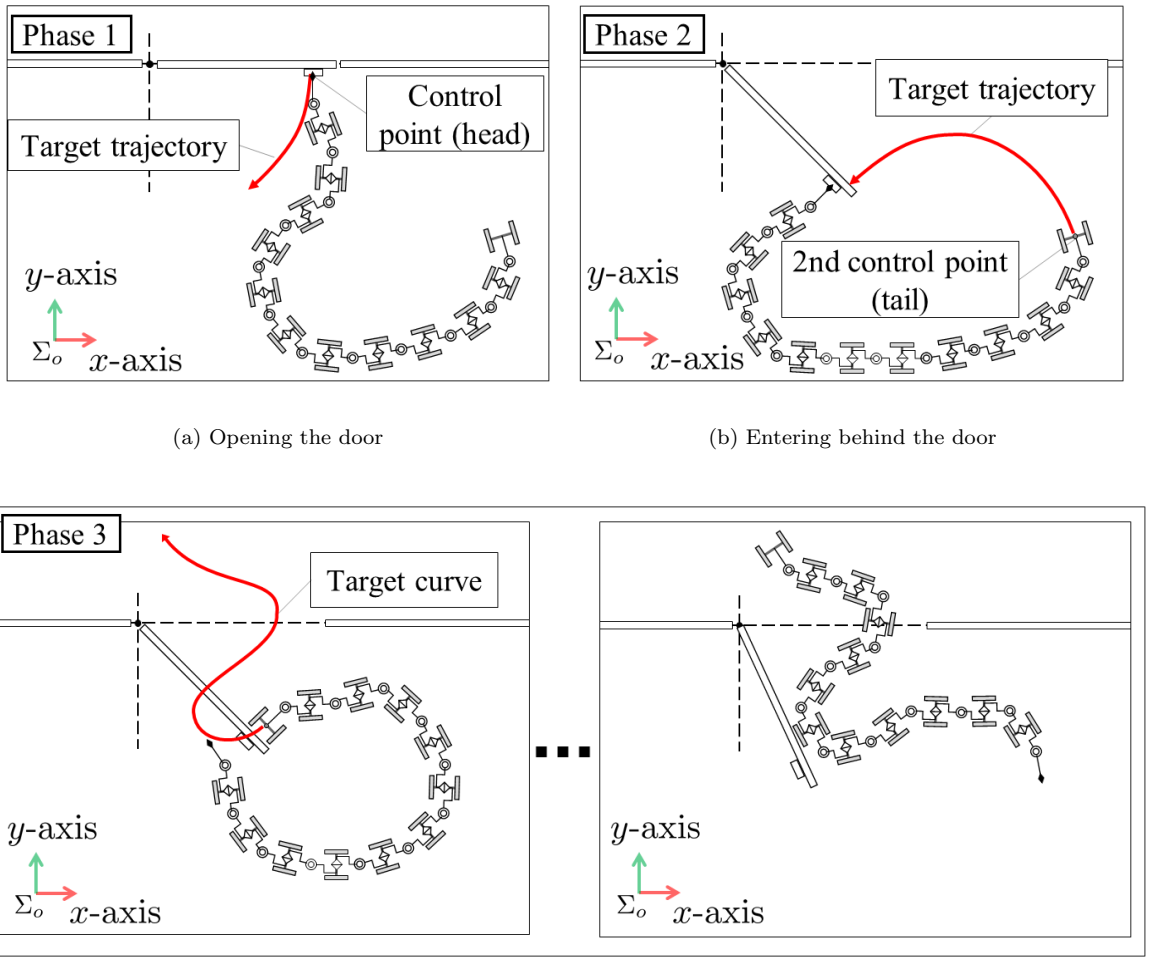

(a) Opening the door

(b) Entering behind the door

(c) Passing through the door

Figure 4. Motion flow

the tail. Finally, the robot passes through the door while pushing the body on the door, keeping the door open (Figure 4(c)). The body shape of the robot is propagated backwards by using the method for approximation to continuous curve [4], and the robot passes through while pushing the body the door.

There is a risk of the robot tipping over when its head is lifted. However, a very large number of joints are necessary to control the two control points simultaneously, and the lifted part is much smaller than the grounded part. Therefore, the risk of the robot tipping over is very low and is ignored in this study. In addition, the maximum spring strength of the door that can be opened by the robot varies greatly depending on the joint torque and the mass and posture of the robot. If the joint torque and the mass of the robot are large, it is expected that the robot will open the strong spring door. To clarify the relationship between the strength of the spring and these parameters, it is necessary to derive the vertical drag forces acting on each wheel. However, these vertical drag forces cannot be uniquely defined, and the maximum spring strength of the door that can be opened by the robot cannot be clarified. The derivation of this relationship is a future work, and the spring of the door is assumed sufficiently small so that the robot can open the door in this study.

4. Kinematic Model

We assume that the grounded wheels do not slip. The kinematic model of the snake robot is obtained by coupling the velocity constraint equations caused by the wheels [15]. The kinematic model for three dimensional motion is also obtained by coupling these velocity constraints and the constraint equation which represents the constraint of the wheel to the ground plane [14], and is represented as

$$\boldsymbol{A}\dot{\boldsymbol{p}}_h = \boldsymbol{B}\dot{\tilde{\boldsymbol{\psi}}} \ , \tag{1}$$

$$\tilde{\boldsymbol{\psi}} = \begin{bmatrix} \boldsymbol{\psi}_h \\ \boldsymbol{\phi}_b \end{bmatrix} \ , \tag{2}$$

where $\boldsymbol{A} \in \mathrm{R}^{n_b+3,6}$, $\boldsymbol{B} \in \mathrm{R}^{n_b+3,2n_h+n_b+1}$. In addition, we introduce the switching constraint [17] into the kinematic model of Eq. (1). By lifting the wheels slightly, the robot operates by switching the velocity constraints. Let σ be a unique identification number that represents the grounded/lifted condition of the wheels, and be called the mode. The mode is determined by solving an optimization problem based on an evaluation function. The detail of the optimization problem is described later. The model will change along with switching mode because the model is derived from the velocity constraints of the grounded wheel. When the mode is σ, the kinematic model is represented as

$$\boldsymbol{A}_\sigma\dot{\boldsymbol{p}}_h = \boldsymbol{B}_\sigma\dot{\tilde{\boldsymbol{\psi}}} \ , \tag{3}$$

where $\boldsymbol{A}_\sigma \in \mathrm{R}^{n_\sigma+3,6}$, $\boldsymbol{B}_\sigma \in \mathrm{R}^{n_\sigma+3,2n_h+n_b+1}$, n_σ is the number of grounded wheels when the mode is σ. In phase 1, $\boldsymbol{p}_h$, the three dimensional position and orientation of the head of the robot is controlled by the kinematic model expressed in Eq. (3).

Next, kinematic model is introduced in phase 2. In phase 2, the three dimensional position and orientation of the head and the tail on the x–y plane are controlled. Let $\tilde{\boldsymbol{p}}_t = \begin{bmatrix} x_t, y_t, Y_t \end{bmatrix}^\top$ be the position and orientation of the tail on the x–y plane. The kinematic relationship between $\tilde{\boldsymbol{p}}_t$, $\boldsymbol{p}_h$, and $\tilde{\boldsymbol{\psi}}$ is represented as

$$\dot{\tilde{\boldsymbol{p}}}_t = \tilde{\boldsymbol{J}}_{t_1}\dot{\boldsymbol{p}}_h + \tilde{\boldsymbol{J}}_{t_2}\dot{\tilde{\boldsymbol{\psi}}} \ , \tag{4}$$

where $\tilde{\boldsymbol{J}}_{t_1} \in \mathrm{R}^{3,6}$, $\tilde{\boldsymbol{J}}_{t_2} \in \mathrm{R}^{3,2n_h+n_b+1}$. The equation coupling Eq. (1) and Eq. (4) is represented as

$$\tilde{\boldsymbol{A}}\dot{\boldsymbol{w}} = \tilde{\boldsymbol{B}}\dot{\tilde{\boldsymbol{\psi}}} \ , \tag{5}$$

$$\tilde{\boldsymbol{A}} = \begin{bmatrix} \boldsymbol{A} & \boldsymbol{O} \\ -\tilde{\boldsymbol{J}}_{t_1} & \boldsymbol{I}_3 \end{bmatrix} \ , \ \tilde{\boldsymbol{B}} = \begin{bmatrix} \boldsymbol{B} \\ \tilde{\boldsymbol{J}}_{t_2} \end{bmatrix} \ , \ \boldsymbol{w} = \begin{bmatrix} \boldsymbol{p}_h \\ \tilde{\boldsymbol{p}}_t \end{bmatrix} \ . \tag{6}$$

As in Eq. (3), we introduce switching constraint into Eq. (5). The equation introducing switching constraint is represented as

$$\tilde{\boldsymbol{A}}_\sigma\dot{\boldsymbol{w}} = \tilde{\boldsymbol{B}}_\sigma\dot{\tilde{\boldsymbol{\psi}}} \ , \tag{7}$$

$$\tilde{\boldsymbol{A}}_\sigma = \begin{bmatrix} \boldsymbol{A}_\sigma & \boldsymbol{O} \\ -\tilde{\boldsymbol{J}}_{t_1} & \boldsymbol{I}_3 \end{bmatrix} \ , \ \tilde{\boldsymbol{B}}_\sigma = \begin{bmatrix} \boldsymbol{B}_\sigma \\ \tilde{\boldsymbol{J}}_{t_2} \end{bmatrix} \ . \tag{8}$$

Eq. (7) is an extended model for two dimensional motion in two-point simultaneous control [24]. In phase 2, $\boldsymbol{w}$, the position and orientation of the head and tail, is controlled using Eq. (7).

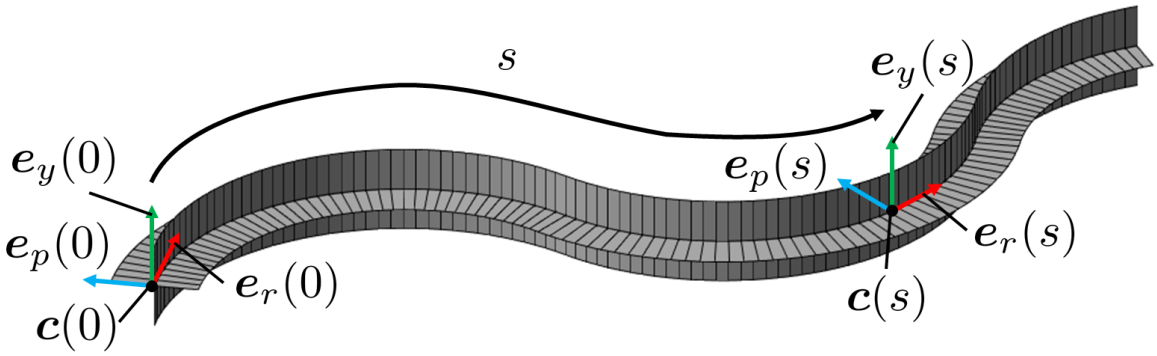

Figure 5. Backbone curve

4.1 *Shape Fitting Motion*

In phase 3, the robot is controlled by using the method of approximation to continuous curve [4]. This method determines the joint angle so that the robot's body shape follows the target continuous curve. The robot propels by changing the target curve like a wave. Considering the joint structure of the robot, the target continuous curve is given as backbone curve, as shown in Figure 5. The backbone curve is defined below as a differential equation.

$$\begin{cases} \frac{d}{ds}\boldsymbol{c}(s) = \boldsymbol{e}_r(s), \\ \frac{d}{ds}\boldsymbol{e}_r(s) = \kappa_y(s)\boldsymbol{e}_p(s) - \kappa_p(s)\boldsymbol{e}_y(s), \\ \frac{d}{ds}\boldsymbol{e}_p(s) = -\kappa_y(s)\boldsymbol{e}_r(s), \\ \frac{d}{ds}\boldsymbol{e}_y(s) = \kappa_p(s)\boldsymbol{e}_r(s), \end{cases} \tag{9}$$

where s represents a position along the target continuous curve, $\boldsymbol{c}(s) = [x(s), y(s), z(s)]^\top$ is the coordinates at point s on a continuous curve, $\boldsymbol{e}_r(s) \in \mathrm{R}^{3,1}$ is the unit vector parallel to the tangent of the curve at s, $\boldsymbol{e}_y(s) \in \mathrm{R}^{3,1}$ is the unit vector which is orthogonal to $\boldsymbol{e}_r(s)$ and pointing upwards in the model at s, $\boldsymbol{e}_p(s) \in \mathrm{R}^{3,1}$ is the unit vector which is represented as $\boldsymbol{e}_p(s) = \boldsymbol{e}_y \times \boldsymbol{e}_r(s)$, $\kappa_y(s)$ and $\kappa_p(s)$ are the curvatures around yaw and pitch axes that determine the shape of the continuous curve. The target backbone curve is determined by $\kappa_y(s)$ and $\kappa_p(s)$. In addition, the lateral rolling locomotion is achieved by rotating $\boldsymbol{e}_p(s)$ and $\boldsymbol{e}_y(s)$ around $\boldsymbol{e}_r(s)$. The detail of this motion is omitted because the rolling motion is not performed in this study.

Let s_h be the position of the head on the continuous curve, $s_i = s_h - il$ be the position of i-th joint on the continuous curve. The body shape is approximated to the interval of $s_h - 2nl \leq s \leq s_h$ of the continuous curve by determining the joint angles with the following equations.

$$\psi_i = -\int_{s_i - l}^{s_i + l} \kappa(s, i)\mathrm{ds}, \tag{10}$$

$$\kappa(s, i) = \begin{cases} \kappa_y(s), & (i : \text{odd}) \\ \kappa_p(s). & (i : \text{even}) \end{cases} \tag{11}$$

By changing the head position s_h, the interval of the curve to be approximated changes, and the motion along the continuous curve is generated. Note that the target continuous curve must be an undulating curve (e.g., serpenoid curve [1]) in order for the propulsion with passive wheels.

Table 1. Conditions for mode

Phase	Mode set	Conditions	$n_{\sigma_{\max}}$
1	ς_1	(i), (ii), (iii), and (iv)	$n + n_h - 2$
2	ς_2	(i), (ii), (iii), (iv), and (v)	$n + n_h - 5$

4.2 *Mode Set*

We introduce the mode σ in phase 1 and 2. The total number of the mode is 2^n when the combination of grounded/lifted conditions of all wheels is considered. However, these modes include modes that are not suitable for operation; e.g., the head part wheels, $1, \cdots, n_h$-th wheels, are always lifted in phase 1, and the tail wheel must be lifted in order to control the position and orientation of the tail in phase 2. Therefore, we introduce the following conditions in order to remove these unsuitable modes.

(i) The robot simultaneously lifts a number fewer than or equal to n_c adjacent pairs of wheels.
(ii) $3 \leq n_\sigma \leq n_{\sigma_{\max}}$.
(iii) $1, \cdots, n_h$-th wheels are lifted.
(iv) $(n_h + 1)$-th wheel is grounded.
(v) n-th wheel is lifted.

The mode which does not satisfy these conditions is not selected. Condition (i) is due to the torque limit of the actual robot [17]. It is difficult to lift many adjacent wheels at the same time because the actual robot has the torque limit of the joint. Therefore, we set the condition (i). Condition (i) must be satisfied in both phase 1 and 2. Condition (ii) is about the number of the grounded wheels, and this condition is caused by the size of the matrices in the kinematic model. The ranks of the model matrices must be full rank to guarantee the convergence of the controlled variables to the target values. The detail of the convergence of the controlled variables to the target values is described later with the control input. Condition (ii) must be satisfied in both phase 1 and 2, but $n_{\sigma_{\max}}$, the maximum number of grounded wheel, is different because each phase has a different model matrix. Conditions (iii) and (iv) are caused by the head raising motion. The head part wheels, $1, \cdots, n_h$-th wheels, are always lifted for raising the head. In addition, $n_h + 1$-th wheel, the first base part wheel, is constrained to the ground plane and must be grounded. Therefore, the conditions (iii) and (iv) must be satisfied in phase 1 and 2 where the robot raises the head. Condition (v) is caused by the control of the tail [24]. If the wheel of the tail is grounded, the velocity constraint interferes the control of the position and orientation of the tail. Thus, n-th wheel, the wheel of the tail, must be lifted. Condition (v) must be satisfied in phase 2 in which the position and orientation of the tail are controlled.

Determining the suitable mode for a situation by searching all the modes that satisfy the conditions is impractical due to the high computational cost. Thus, by selecting a suitable mode from the mode set which consists of the mode picked out from modes that satisfy the constraints, the computational cost is reduced and the real-time control is achieved. Let ς_1 and ς_2 be the mode set in each phase. Table 1 shows the correspondence between each phase and the conditions to be satisfied and the mode set. $n_{\sigma,\max}$ is determined depending on the model matrix in each phase, and the details will be described later.

5. Controller Design

Figure 6 shows the schematic diagram of the controller, and Table 2 shows the correspondence between blocks in Fig. 6 and the equations used in each phase. Initially, the controller corresponding to each phase is selected (Fig. 6 Selecting controller block). In phase 1 and 2, a suitable mode for the situation is then selected from ς_i $(i = 1, 2)$, which is the mode set in each phase (Fig. 6 Selecting mode block). The mode is selected by solving an optimization problem at regular

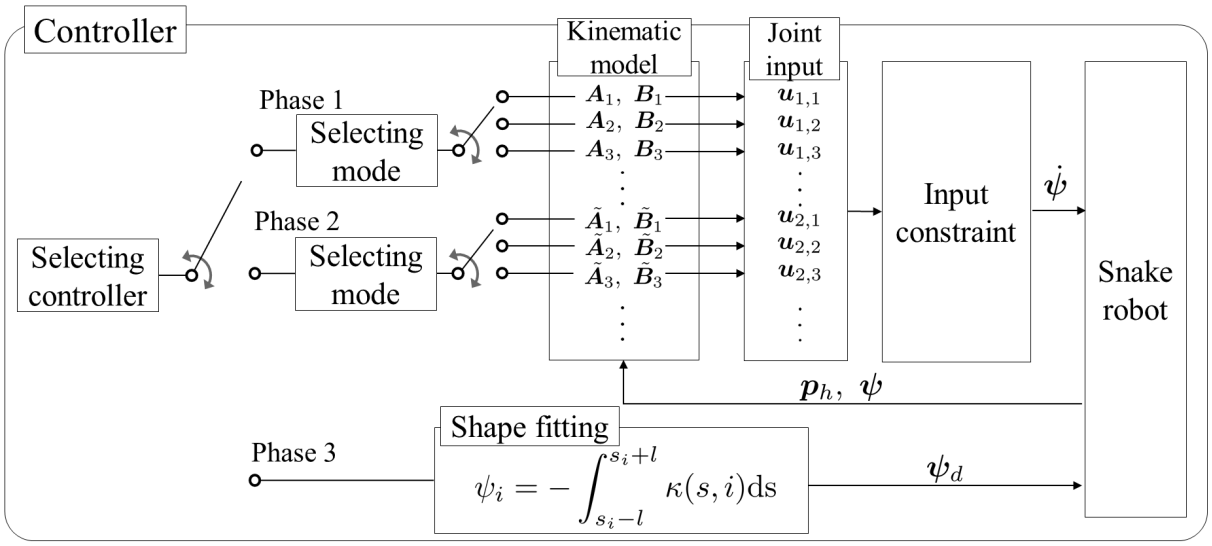

Figure 6. Controller

Table 2. Summary of the controller

Phase	Eq. of model	Eq. of input	Controlled variable	Mode set
1	Eq. (1)	Eq. (12)	$\boldsymbol{p}_h$	ς_1
2	Eq. (5)	Eq. (12)	$\boldsymbol{p}_h$ and $\tilde{\boldsymbol{p}}_t$	ς_2
3	Eq. (9)	Eq. (10)	-	-

intervals and maintained until the next switch. The control model is determined by the selected mode (Fig. 6 Kinematic model block). The joint inputs for converging the controlled variables to the target values are calculated with the determined model (Fig. 6 Joint input block). In this block, we aim to realize subtasks using the kinematic redundancy of the robot. The calculated input is constrained by the input constraint (Fig. 6 Input constraint). If the norm of the input is excessive, the input constraint sets the input to zero, and prevents unexpected motion which occurs when the robot is near the singular posture. In phase 3, the joint angles are determined for fitting the body to target continuous curve from Eq. (10).

5.1 *Joint Input*

In phase 1 and 2, the joint input for converging the controlled variables to the target values is calculated using each kinematic model. In phase 3, the target joint angles are determined based on Eq. (10) and the robot is controlled. We show only the input calculation in phase 2 because the input calculation in phase 1 and 2 are similar. Based on Eq. (5), the joint input $\boldsymbol{u}_\sigma = \dot{\tilde{\boldsymbol{\psi}}}$ is calculated as

$$\boldsymbol{u}_\sigma = \boldsymbol{u}_{\sigma,c} + \boldsymbol{u}_{\sigma,\mathrm{ker}} \ , \tag{12}$$

$$\boldsymbol{u}_{\sigma,c} = \tilde{\boldsymbol{B}}_\sigma^\dagger \tilde{\boldsymbol{A}}_\sigma \left\{ \dot{\boldsymbol{w}}_d + \boldsymbol{K}_p \left(\boldsymbol{w}_d - \boldsymbol{w} \right) \right\} \ , \tag{13}$$

$$\boldsymbol{u}_{\sigma,\mathrm{ker}} = k_v \left(\boldsymbol{I} - \tilde{\boldsymbol{B}}_\sigma^\dagger \tilde{\boldsymbol{B}}_\sigma \right) \boldsymbol{\eta} \ , \tag{14}$$

$$\boldsymbol{\eta} = \left[\frac{\partial V}{\partial \tilde{\psi}_1}, \cdots, \frac{\partial V}{\partial \tilde{\psi}_{\tilde{n}}} \right]^\top \ , \tag{15}$$

where $\tilde{\boldsymbol{B}}_\sigma^\dagger$ is the pseudo inverse matrix of $\tilde{\boldsymbol{B}}_\sigma$, $\boldsymbol{K}_p$ is the control gain for the controlled variables, $k_v \geq 0$ is the gain for the input using redundancy, $\boldsymbol{u}_{\sigma,\mathrm{ker}}$ is the input due to redundancy. The time derivative of the evaluation function $V(\boldsymbol{q})$ is represented as

$$\begin{aligned}\frac{dV}{dt} &= \frac{\partial V}{\partial \boldsymbol{p}_h}\dot{\boldsymbol{p}}_h + \frac{\partial V}{\partial \tilde{\boldsymbol{\psi}}}\dot{\tilde{\boldsymbol{\psi}}} \\ &= \frac{\partial V}{\partial \boldsymbol{p}_h}\dot{\boldsymbol{p}}_h + \boldsymbol{\eta}^\top \boldsymbol{u}_{\sigma,c} + k_v \boldsymbol{\eta}^\top (\boldsymbol{I} - \tilde{\boldsymbol{B}}_\sigma^\dagger \tilde{\boldsymbol{B}}_\sigma)\boldsymbol{\eta}. \end{aligned} \tag{16}$$

The third term on the right hand side of Eq. (16) is non-negative and $\boldsymbol{u}_{\sigma,\mathrm{ker}}$ is expected to increase V. The detail of V is described later. If $\tilde{\boldsymbol{B}}_\sigma$ is a full row rank, $\tilde{\boldsymbol{B}}_\sigma \tilde{\boldsymbol{B}}_\sigma^\dagger = \boldsymbol{I}$. The closed loop of the system is represented as

$$\tilde{\boldsymbol{A}}_\sigma \left\{ \dot{\boldsymbol{w}}_d - \dot{\boldsymbol{w}} + \boldsymbol{K}_p \left(\boldsymbol{w}_d - \boldsymbol{w} \right) \right\} = \boldsymbol{0} \ . \tag{17}$$

If $\tilde{\boldsymbol{A}}_\sigma$ is a full column rank, the controlled variables $\boldsymbol{w}$ converge to the target value $\boldsymbol{w}_d$ when $t \to \infty$.

In contrast, if $\tilde{\boldsymbol{A}}_\sigma$ or $\tilde{\boldsymbol{B}}_\sigma$ is not a full rank, the convergence of controlled variables to the target value is not guaranteed. We call such configurations the singular configurations. Therefore, $\tilde{\boldsymbol{A}}_\sigma$ and $\tilde{\boldsymbol{B}}_\sigma$ must be full rank for converging the controlled variables to the target value. The singular configurations due to $\tilde{\boldsymbol{A}}_\sigma$ and $\tilde{\boldsymbol{B}}_\sigma$ are called singular configuration I and II, respectively. When the robot's posture is the singular configuration I, the motion of the robot is not uniquely defined, and the robot does not move according to the target. When the robot's posture is similar to the singular configuration II, the input becomes excessive and the robot shows unexpected behavior. In Phase 1, the size of $\boldsymbol{B}_\sigma$ is $\boldsymbol{B}_\sigma \in \mathrm{R}^{n_\sigma+3, n+n_h+1}$, and n_σ needs to satisfy $n_\sigma + 3 \leq n + n_h + 1$ because $\boldsymbol{B}_\sigma$ is full row rank. Thus, $n_{\sigma,\max} = n + n_h - 2$ in Phase 1. Similarly, the size of $\tilde{\boldsymbol{B}}_\sigma$ is $\tilde{\boldsymbol{B}}_\sigma \in \mathrm{R}^{n_\sigma+6, n+n_h+1}$, and $n_{\sigma,\max} = n + n_h - 5$ in Phase 2.

5.2 *Selecting Mode*

The mode is selected by solving an optimization problem [17]. The mode is selected at regular intervals and the mode at t is represented as

$$\sigma(t) = \sigma_k \ , \ (t_k \leq t < t_k + 1) \tag{18}$$

$$t_k = k t_\sigma \ , \ (k = 0, 1, \cdots) \tag{19}$$

where $t_\sigma > 0$ is a constant that represents the cycle of the mode switching. The mode σ_k is determined by solving the following optimization problem at $t = k t_\sigma$.

$$\max_{\sigma_k} \ J, \tag{20}$$

$$J = \varphi\left(\hat{\boldsymbol{q}}\left(t_p, \sigma_k\right)\right) + \int_{t_k}^{t_p} \Gamma\left(\hat{\boldsymbol{q}}\left(\tau, \sigma_k\right), \boldsymbol{u}_{\sigma_k}\left(\tau, \sigma_k\right)\right) d\tau, \tag{21}$$

where $\hat{\boldsymbol{q}}$ is the estimation value of $\boldsymbol{q}$, and t_p is the predictive horizon. φ and Γ are the evaluation function for selecting the mode. If the input becomes excessive in the prediction interval due to the singular configuration II, its mode is excluded from selection. If the input becomes excessive in all modes, the mode is selected based on optimization problem from among the modes which remain the last. We set $\varphi = V(\boldsymbol{q})$, $\Gamma = 0$, and $t_p = t_{k+1}$. $V(\boldsymbol{q})$ is the evaluation function for the redundancy of joint and its detail is described later. $\hat{\boldsymbol{q}}$ is calculated using the kinematic model and the closed loop system.

5.3 *Input Constraint*

When the robot is controlled using the two-point simultaneous control method, the input becomes excessive if the robot posture is similar to the singular configuration II [24]. It is difficult to avoid the singular configuration completely because it also depends on the target value of the controlled variables, even if the singular avoidance using kinematic redundancy is implemented. Thus, we introduce the following input constraint as well [24].

$$\boldsymbol{u}_\sigma = \begin{cases} \boldsymbol{0}, & (\text{if } ||\boldsymbol{u}_\sigma|| > u_{\lim}) \\ \boldsymbol{u}_\sigma, & (\text{otherwise}) \end{cases} \tag{22}$$

where $u_{\lim}$ is the threshold for the input constraint. If the input exceeds the threshold $u_{\lim}$, the input becomes the zero and the robot stops. The singular configuration changes depending on the grounded/lifted state of the wheels, i.e. the mode σ, and the mode is selected with reference to the value of the evaluation function. Therefore, by considering the singular configuration in the evaluation function, the robot can restart along with switching the mode. The robot cannot restart if it becomes the singular configuration in all modes, but it can be avoided by appropriate setting.

5.4 *Evaluation Function*

We aim to realize the subtasks with redundancy by designing the evaluation function V based on subtasks. The evaluation function V is represented as the weighted sum of the evaluation function of each subtask. The subtasks are represented as

(1) Avoidance of the joint limits,
(2) Singular avoidance,

Considering the subtasks, the evaluation function is represented as

$$V = \boldsymbol{w}_v \left[V_1 \; V_2 \; V_3 \right]^\top , \tag{23}$$

$$V_1 = -\sum_{k=1}^{2n-1} f\left(c_{\psi,i}, |\psi_k|\right), \tag{24}$$

$$V_2 = \det\left(\boldsymbol{A}_p^\top \boldsymbol{A}_p\right), \tag{25}$$

$$V_3 = \det\left(\boldsymbol{B}_p \boldsymbol{B}_p^\top\right), \tag{26}$$

$$\boldsymbol{A}_p = \begin{cases} \boldsymbol{A}_\sigma, & (\text{phase} : 1) \\ \tilde{\boldsymbol{A}}_\sigma, & (\text{phase} : 2) \end{cases} \tag{27}$$

$$\boldsymbol{B}_p = \begin{cases} \boldsymbol{B}_\sigma, & (\text{phase} : 1) \\ \tilde{\boldsymbol{B}}_\sigma, & (\text{phase} : 2) \end{cases} \tag{28}$$

$$f(x,y) = \begin{cases} (y-x)^2, & (\text{if } x < y) \\ 0, & (\text{otherwise}) \end{cases} \tag{29}$$

$$c_{\psi,i} = \begin{cases} c_{\psi,y}, & (i : \text{odd}) \\ c_{\psi,p}, & (i : \text{even}) \end{cases} \tag{30}$$

where $\boldsymbol{w}_v \in \mathrm{R}^{1,3}$ is the weight for the each evaluation function. $c_{\psi,i}$ is a threshold value for

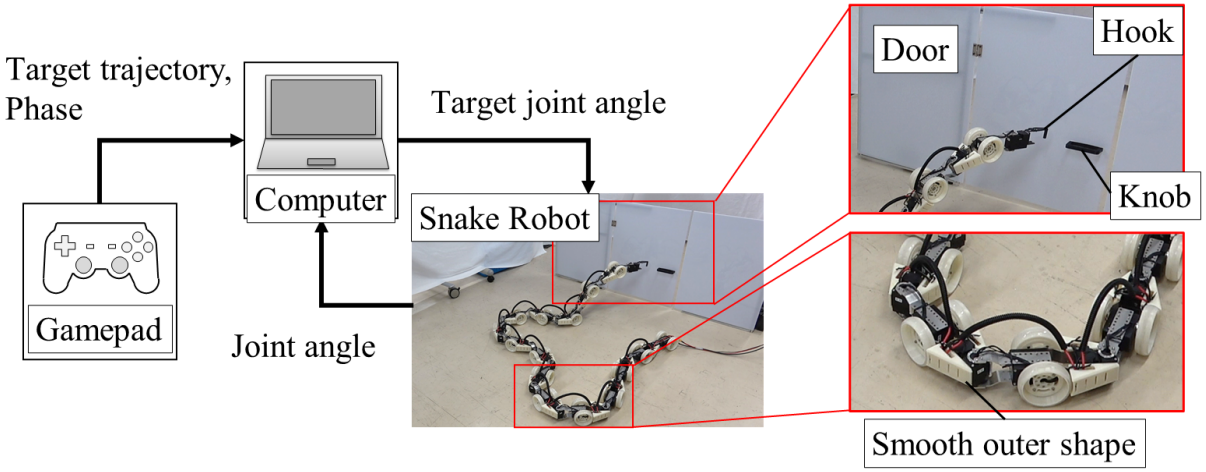

Figure 7. Experimental environment

avoiding joint limits, and it is an arbitrary constant. $c_{\psi,y}$ and $c_{\psi,p}$ are the threshold values for the yaw joints and pitch joints, respectively. V_1 is the function for avoidance of the joint limits, V_2 and V_3 are the function for the singular avoidance. The function $f(x, y)$ sets the dead zone of the joint angle in V_1. $|\psi_i|$ must not reach the angle limit, but it need not be as small as approximately zero. If $|\psi_i|$ does not exceed the threshold value $c_{\psi,i}$, $f\left(c_{\psi,i}, |\psi_i|\right)$ becomes zero, and the other subtasks are prioritized. When $|\psi_i|$ exceeds the threshold value $c_{\psi,i}$, V_1 increases suddenly and the avoidance of the joint angle limit is prioritized over the other subtasks. These functions are same as in [24] and the avoidance of the joint limits and the singular avoidance can be expected by increasing the evaluation function. The weights for each evaluation function are determined by trial and error.

The proposed method only contributes to the increase in the evaluation function, but does not guarantee it. Therefore, the evaluation function may decrease depending on $\boldsymbol{u}_{\sigma,c}$, the input related to the convergence of the controlled variables to the target value. One way to avoid this problem is to stop the operation of the control points temporarily. In this case, an increase in the evaluation function is guaranteed because $\boldsymbol{u}_{\sigma,c} = \boldsymbol{0}$. Thus, by temporarily stopping the control points, it is expected that fatal problems, such as the joint exceeding the angle limit or the posture of the robot becoming very close to the singular configuration, are avoided. In addition, $\boldsymbol{u}_{\sigma,c}$ becomes small when the control points move slowly, which improves the possibility of an increase in the evaluation function.

6. Experiments

The effectiveness of the proposed method was verified by the experiments. Figure 7 shows the experimental environment and the snake robot which was used in the experiment. The robot was constructed using the serial-controlled servo motors XM540-W270-R (Dynamixel, Robotis, Inc.) and passive wheels. The present angles can be obtained from the motors through a serial communication from the computer. The passive wheels are made of silicon, and their coefficient of friction is sufficiently large to satisfy the velocity constraint. In addition, the robot has a smooth outer shape that prevents it from becoming stuck at the door. If the body shape at the rear part of the wheel is not smooth, as shown in Figure 8(a), the robot becomes stuck through a collision with the edge of the door in Phase 3. The smooth shape shown in Fig. 8(b) prevents the robot from becoming stuck because the edge of the door slides along the body shape. The environment was assumed to be unknown, the absolute position and orientation of the door and the robot could not be measured, and the target values of the controlled variables

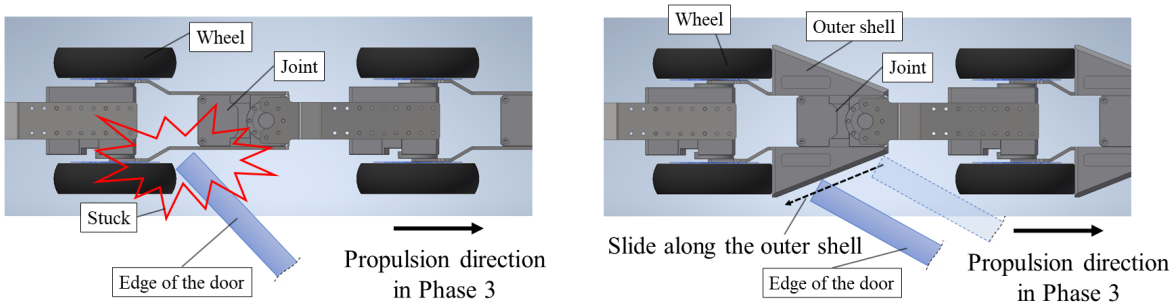

(a) Without outer shell (b) With outer shell

Figure 8. Stuck due to the collision between the robot and the edge of the door

Table 3. Mode sets and allocations of grounded/lifted wheels

Mode set	n_σ	Wheel num. (L: lifted, G: grounded)														
		1	2	3	4	5	6	7	8	9	10	11	12	13	14	15
ς_1	8	L	L	G	G	G	L	G	G	L	L	G	G	L	L	G
		L	L	G	G	G	L	G	L	G	L	G	L	G	L	G
		L	L	G	G	G	L	L	G	G	L	L	G	G	L	G
		L	L	G	G	L	G	G	L	L	G	G	L	L	G	G
		L	L	G	G	L	G	L	G	L	G	L	G	L	G	G
ς_2	6	L	L	G	L	L	G	G	L	G	L	G	L	G	L	L
		L	L	G	G	L	G	L	G	L	L	G	L	L	G	L
		L	L	G	L	L	G	G	L	G	L	G	L	L	G	L
		L	L	G	L	L	G	L	L	G	G	L	G	L	G	L
		L	L	G	L	L	G	L	L	G	L	G	G	L	G	L

and the timing of the switching phase were determined by operator by using gamepad. The number of wheel is $n = 15$, the length of link is 0.0985 m, the radius of the wheel is 0.04 m. The joint angle limits of the yaw and pitch joint are $5\pi/9$ rad and $2\pi/3$ rad, respectively. The width and height of the door are 0.47 m and 0.62 m, respectively, the mounting height of the knob is 0.25 m, and the force required to open the door is approximately 2.0 N. This force value is sufficiently small for the robot to open the door. The joint angles were measured from the actuator. The position and orientation of the head were estimated from the input and the closed loop system. We set the parameters of controller as $K_p = \mathbf{0}$, $k_v = 1.0$, $t_\sigma = 1.0$ s, $u_{\lim} = 2.0$, $c_{\phi,y} = 10\pi/27$, and $c_{\phi,p} = 4\pi/9$. The weights of the evaluation function in phase 1 and 2 was $\boldsymbol{w}_v = [1.5,\ 2.0 \times 10^{-3},\ 3.0 \times 10^{8}]$. The control cycle was $t_s = 0.10$. w_v was adjusted so that the orders of all the evaluation functions were close to each other based on their time response in the numerical simulation and preliminary experiment. Each evaluation function changes suddenly when it needs to act preferentially. Therefore, if the weight w_v is adjusted so that the orders of the evaluation functions are close to each other in the normal state, each evaluation function acts preferentially when it is required (e.g., when the joint angles are close to the angle limit). The mode sets in each phase consist of five modes selected from all modes that satisfy the conditions. Table 3 shows the grounded/lifted state of each mode. The number of mode candidates was determined based on the constraint of the control cycle. We set the number of mode candidates as large as possible within the range in which calculations can be performed in real time. The mode candidates were selected so that each candidate was as different as possible. The initial posture

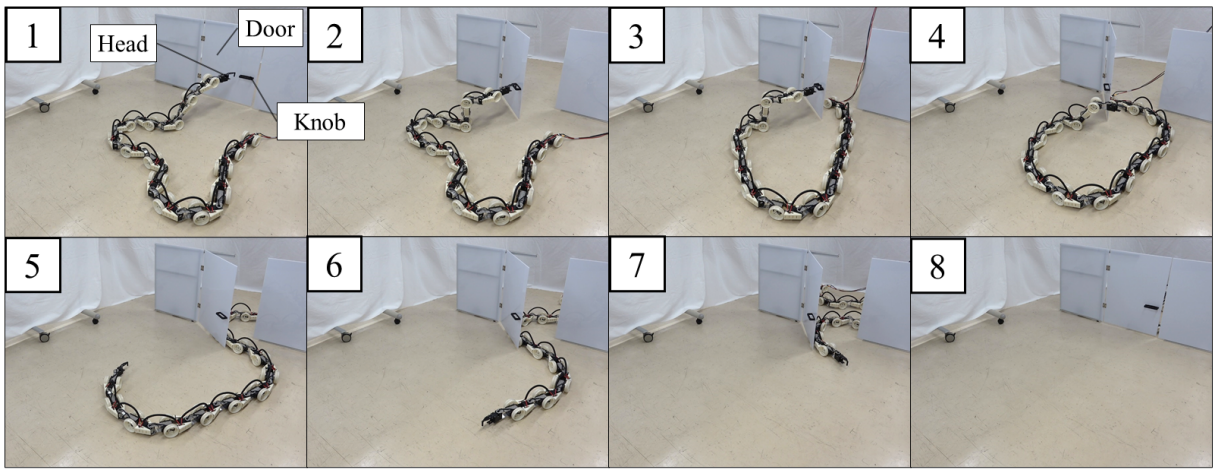

(a) The motion of the robot

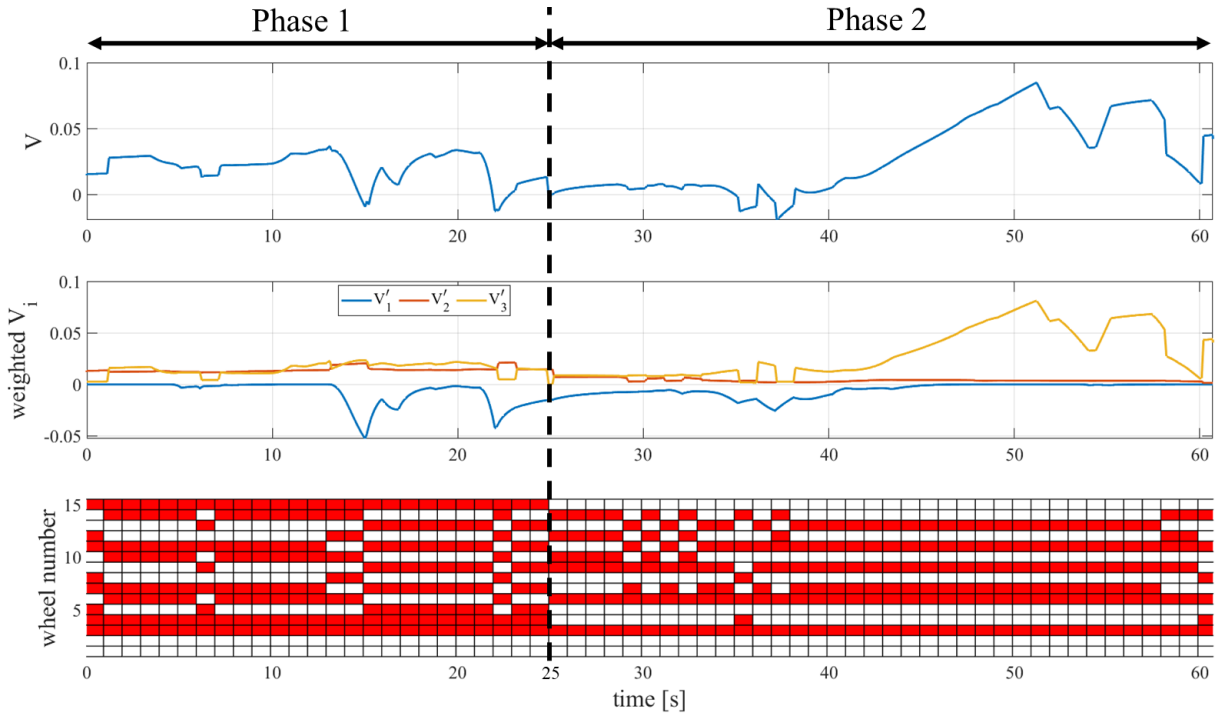

(b) Time response of the cost function and the grounded/lifted state of each wheel

Figure 9. Experimental result

of the robot was determined based on numerical simulations and preliminary experiments. The head and tail of the robot are control points that approach the door. Therefore, as shown in Fig. 7, the posture in which these control points face the door is desirable. If the tail of the robot is away from the door in the initial posture, the tail has to approach the door in Phase 2, which takes a very long time. To change the initial posture to an appropriate one, a method that changes the posture of the robot to an arbitrary posture while fixing the head position has been proposed [18]. This method allows the robot to transform into a posture suitable for opening the door. In this experiment, the initial posture was set to the appropriate posture, and

the transition to the initial posture was omitted.

Figure 9 shows the experimental results. The time response of the joint angle is omitted because all the joint angles were below the limit. Fig. 9(a) and Fig. 9(b) shows the motion of the robot and the time responses of the evaluation functions and the selected mode, respectively. V_i' $(i = 1, \cdots, 3)$ in Fig. 9(b) is V_i multiplied by the weights. The red and white squares in Fig. 9(b) represent the grounded and lifted wheel, respectively. From Fig. 9, the robot entered through the door by using the proposed method. By controlling the head and tail simultaneously, the robot entered through, tail first while keeping the door open (Fig. 9 3–4). In addition, the smooth body shape prevented the robot from the stack caused by the collision between the edge of the door and the robot (Fig. 9 5–8).

In Fig. 9(b), the robot was moving while switching the mode. The discrete changes in the evaluation functions depend on the switching of the referenced model matrix. From the time responses of the evaluation functions in Fig. 9(b), V_3 increased in phase 2. In addition, the excessive input caused by the singular configuration II did not occur and the robot moved continuously. In contrast, V_2 was smaller value in phase 2, but this is not a fatal problem since the robot can move continuously if V_2 is non-zero. The minimum value of V_2 was 0.72, but the robot's posture did not become singular configuration I. Thus, it was verified that the robot can pass through a self-closing door without the stack caused by collision between the robot and the edge of the door.

However, the force which acts on the robot by the door is not considered. If the spring of the hinge is very strong or the robot is very light compared to the door, the robot is in danger of failing to pass through the door because of the skidding of the robot. The motion considering the external force acting on the robot is an issue for future work.

7. Conclusion

We proposed the control method for a snake robot to pass through a self-closing door, using the two-point simultaneous control method [24]. The proposed method enables the robot to pass through a self-closing door while keeping the door open by controlling the head and tail simultaneously. In addition, the smooth body shape prevents the robot from the stack which is caused by the collision between the edge of door and the robot. The experiments demonstrated the effectiveness of the proposed method, and the robot passed through the simplified self-closing door. In future works, we will work on the motion considering the external force acting on the robot.

Acknowledgment

We would like to thank Editage (www.editage.com) for English language editing.

References

[1] Hirose S. Biologically Inspired Robots (Snake-like Locomotor and Manipulator). Oxford University Press. 1993.
[2] Crespi A, Ijspeert AJ. Online optimization of swimming and crawling in an amphibious snake robot. IEEE Trans Robotics. 2008;24(1):75–87.
[3] Wu X, Ma S. Neurally Controlled Steering for Collision-Free Behavior of a Snake Robot. IEEE Trans Control Systems Technology. 2013;21(6):2443–2449.
[4] Yamada H, Hirose S. Study of active cord mechanism: approximations to continuous curves of a multi-joint body (Japanese). Journal of Robotics Society of Japan. 2008;26(1):110–120.
[5] Kamegawa T, Harada T, Gofuku A. Realization of cylinder climbing locomotion with helical form

by a snake robot with passive wheels. In: Proc. IEEE Int. Conf. Robotics and Automation. 2009. p. 3067–3072.
[6] Kamegawa T, Baba T, Gofuku A. V-shift control for snake robot moving the inside of a pipe with helical rolling motion. In: Proc. IEEE Int. Symp. on Safety, Security and Rescue Robotics. 2011. p. 1–6.
[7] Qi W, Kamegawa T, Gofuku A. Helical wave propagation motion for a snake robot on a vertical pipe containing a branch. Journal of Artificial Life and Robotics. 2018;23(4):515–522.
[8] Takemori T, Tanaka M, Matsuno F. Gait Design of a Snake Robot by Connecting Curve Segments and Experimental Demonstration. IEEE Trans Robotics. 2018;34(5):1384–1391.
[9] Takemori T, Tanaka M, Matsuno F. Ladder Climbing with a Snake Robot. In: Proc. IEEE/RSJ Int. Conf. Intelligent Robots and Systems. 2018. p. 1–9.
[10] Hatton RL, Choset H. Generating gaits for snake robots: annealed chain fitting and keyframe wave extraction. Autonomous Robots. 2010;28(3):271–281.
[11] Rollinson D, Choset H. Pipe Network Locomotion with a Snake Robot. Journal of Field Robotics. 2016;33(3):332–336.
[12] Gong C, Tesch M, Rollinson D, Choset H. Snakes on an Inclined Plane: Learning an adaptive sidewinding motion for changing slopes. In: Proc. IEEE Int. Conf. on Intelligent Robots and Systems. 2013. p. 1114–1119.
[13] Prautsch P, Mita T, Iwasaki T. Analysis and control of a gait of snake robot. IEEJ Trans Industry Applications. 2000;120(3):372–381.
[14] Tanaka M, Matsuno F. Modeling and control of head raising snake robots by using kinematic redundancy. Journal of Intelligent and Robotic Systems. 2014;75(1):53–69.
[15] Matsuno F, Mogi K. Redundancy Controllable System and Control of Snake Robot with Redundancy based on Kinematic Model. In: Proc. IEEE Int. Conf. Decision and Control. 2000. p. 4791–4796.
[16] Tanaka M, Kon K, Tanaka K. Range-sensor-based Semiautonomous Whole-body Collision Avoidance of a Snake Robot. IEEE Trans on Control Systems Technology. 2015;23(5):1927–1934.
[17] Tanaka M, Matsuno F. Control of Snake Robots with Switching Constraints: trajectory tracking with moving obstacle. Advanced Robotics. 2014;28(6):415–429.
[18] Tanaka M, Tanaka K. Shape Control of a Snake Robot with Joint Limit and Self-collision Avoidance. IEEE Trans Control Systems Technology. 2017;25(4):1441–1448.
[19] Mohammadi A, Rezapour E, Maggiore M, Pettersen KY. Maneuvering Control of Planar Snake Robots Using Virtual Holonomic Constraints. IEEE Trans Control Systems Technology. 2016; 24(3):884–899.
[20] Transeth AA, Leine RI, Glocker C, Pettersen KY, Liljebäck P. Snake Robot Obstacle-Aided Locomotion: Modeling, Simulations, and Experiments. IEEE Trans on Robotics. 2008;24(1):88–104.
[21] Liljebäck P, Pettersen KY, Stavdahl Ø, Gravdahl JT. Snake Robot Locomotion in Environments With Obstacles. IEEE/ASME Trans on Mechatronics. 2012;17(6):1158–1169.
[22] Tanaka M, Tadakuma K, Nakajima M, Fujita M. Task-Space Control of Articulated Mobile Robots With a Soft Gripper for Operations. IEEE Trans on Robotics. 2018;35(1):135–146.
[23] Sverdrup-Thygeson J, Kelasidi E, Pettersen KY, Gravdahl JT. The Underwater Swimming Manipulator–A Bioinspired Solution for Subsea Operations. IEEE Journal Oceanic Engineering. 2018;43(2):402–417.
[24] Nakajima M, Tanaka M, Tanaka K. Simultaneous Control of Two Points for Snake Robot and Its Application to Transportation. IEEE Robotics and Automation Letters. 2020;5(1):111–118.
[25] Nakajima M, Tanaka M, Tanaka K. Motion design of a snake robot to pass through a door. In: Proc. The Third Int. Symp. Swarm Behavior and Bio-Inspired Robotics. 2019. p. 205–207.
[26] Farelo F, Alqasemi R, Dubey R. Task-oriented control of a 9-DoF WMRA system for opening a spring-loaded door task. In: IEEE Int. Conf. Rehabilitation Robotics. 2011. p. 1–6.
[27] Axelrod B, Huang WH. Autonomous door opening and traversal. In: IEEE Int. Conf. Technologies for Practical Robot Applications (TePRA). 2015. p. 1–6.